ACS APPLIED MATERIALS & INTERFACES

www.acsami.org

Research Article

Multicolor Conjugated Polymer Thin Films with Tunable Responsivity to Oxidative and Reductive Environments

Ji-eun Park, Soomin Lee, Youngji Kim, Shine K. Albert, Yumin Lee, Jerome Kartham Hyun,* Wooyoung Lee,* and So-Jung Park*

Cite This: *ACS Appl. Mater. Interfaces* 2023, 15, 51753−51762

Read Online

ACCESS | Metrics & More | Article Recommendations | Supporting Information

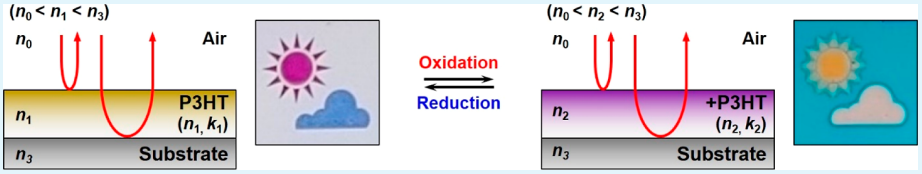

ABSTRACT: Dynamic colors that respond to environmental changes are of great interest for diverse areas of science and technology ranging from chemical and biological sensors to smart information display. Here, we demonstrate a multitude of responsive colors from a conjugated polymer film arising from a thin-film interference. This mechanism provides an excellent control over the thin-film color by varying the film thickness, type of substrate, and degree of polaron population and is generally applicable to various conjugated polymers for further color variation. Furthermore, multiple sets of responsive colors are achieved from a single polymer layer by patterning the underlying substrate to spatially modify the interference conditions. Using this system, we demonstrate the reversible color changes induced by an oxidative or reductive environment with color responsivity controllable with the nature of the polaron state.

KEYWORDS: *thin-film interference, structural color, stimuli-responsive, conjugated polymer, hole polaron*

INTRODUCTION

Nature displays numerous examples of variable coloration for camouflage and communication.[1−4] Adaptation of such responsive colors in our living can provide a real-time visible signal for environmental changes, useful for a number of applications such as smart information display, encryption, and sensors.[5−10] Among various color-changing materials,[5,7,9,11,12] the conjugated polymers are of particular interests for their tunable optical and electrical properties and low-cost solution processability.[12−20] The conjugated polymers are intensely colored in the neutral state due to strong light absorption in the visible region. Upon oxidation, the absorption shifts to longer wavelengths typically in the near-infrared (IR) region, resulting in color bleaching or change.[20−24] This optical property is responsible for the electrochromic behavior of the conjugated polymers, which has been utilized in various applications such as smart windows and electronic skin.[6,8,25] However, the possible colors from a conjugated polymer are usually limited to two states with varying intensities when the coloration mechanism is based on the intrinsic absorption property,[20] and further color tuning requires the design and synthesis of new polymers with different molecular structures.

Here, we realize a wide range of responsive colors by adopting conjugated polymers to exhibit a simple thin-film interference. The thin-film interference color, which is commonly seen in soap bubbles and oil films, is based on the constructive and destructive interferences between light reflected from the top and bottom of the films. We have previously shown that the oxidative liquid−liquid interfacial self-assembly of a conjugated block copolymer, poly(3-hexylthiophene)-*block*-poly(ethylene glycol) (P3HT-*b*-PEG), can generate an oxidized P3HT-*b*-PEG film displaying colorimetric sensitivity to reductive vapors via the thin-film interference.[24] While this method provided a one-step procedure to prepare an oxidized polymer film, the color tunability was limited as the degree of oxidation and the film thickness, two key parameters for color modulation, could not be independently controlled in the in situ oxidation method. Herein, we demonstrate full color tunability from a conjugated polymer by decoupling the oxidation and the film formation through a simple spin-coating and postoxidation process, which is generally applicable to commercially available prototypical conjugated polymers. A range of different color combinations and color patterns with varying responsivities to reductive and oxidative species were achieved by the combination of film thickness, type of substrate, and reduction

Received: August 11, 2023
Revised: October 6, 2023
Accepted: October 18, 2023
Published: October 30, 2023

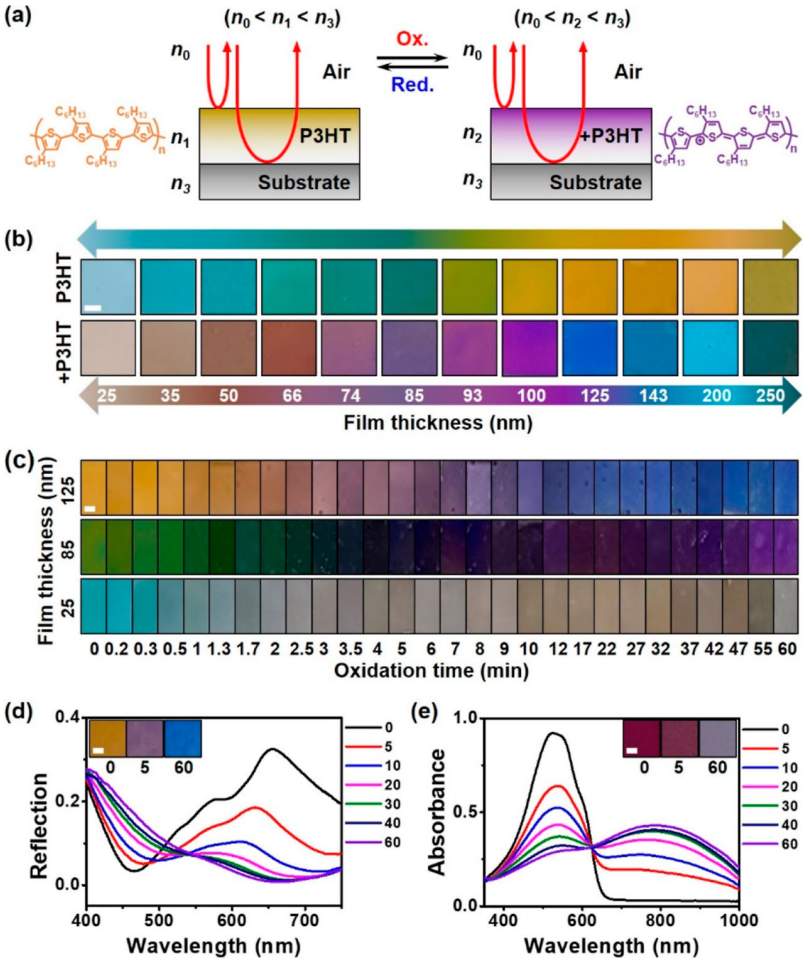

Figure 1. Working principle and optical characterization of the tunable thin-film interference display. (a) Schematic of the tunable structural color principle via the thin-film interference through the material change depending on their oxidation state. (b) Color obtained by tuning the thickness (t) of P3HT and +P3HT films on Si substrate (scale bar: 1 mm). (c) Photographs showing color pallet of the P3HT films depending on the film thickness and the oxidation time with a 100 μM $HAuCl_4$ solution (scale bar: 1 mm). (d,e) Time-dependent reflection (d) and UV−vis (e) spectra of the P3HT film oxidation reaction (scale bar: 2 mm). The P3HT film was dipped in a 100 μM $HAuCl_4$ solution. Each subsequent scan occurred at 5, 10, 20, 30, 40, and 60 min.

potential of oxidants. The superior versatility, robustness, and generality of conjugated polymer-based responsive thin-film interference colors make them highly suitable for colorimetric sensors and smart label applications beyond previous electrochromic research based on the absorption color.

RESULTS AND DISCUSSION

Tunable Thin-Film Interference Color of the P3HT Film. Figure 1a presents a schematic of our responsive thin-film interference color system composed of a conjugated polymer layer on a reflective substrate. In our typical study, the thin-film interference color was fabricated by spin-coating a 1,4-dichlorobenzene solution of P3HT on a silicon wafer, where the film thickness was controlled by simply varying the polymer concentration. P3HT was selected as our typical thin-film material for the large contrast in optical constant it possesses between oxidized and neutral states, making the colors dynamically switchable. Figure 1b (top) presents photographs of P3HT thin films of varying thickness (Tables S1 and S2, Figure S1), exhibiting thin-film interference colors varying with the film thickness. As mentioned above, these colors originate from the interference between light normally reflected by the top and bottom interfaces. Due to the larger index of each underlying layer, the light is reflected at each interface with a near π-phase shift. This results in strengthening of the total reflected light when integer multiples of its half wavelength in the polymer correspond to the polymer thickness. As a result, the modulated spectrum varies with thickness, the effect of which is illustrated in Figure 1b (top) via the display of various structural colors.

The color-switching capability of P3HT thin films (Figure 1a) was assessed by exposing the film to a $HAuCl_4$ (500 μM) solution for 1 min to generate oxidized P3HT (+P3HT). Consistent with the literatures,[26−28] the cyclic voltammetry data of P3HT revealed reversible oxidation and reduction, with the estimated highest occupied molecular orbital (HOMO) energy of −4.82 eV (Figure S2). The comparison of the HOMO level and the reduction potential of Au^{3+} (Figure S3) indicates that the hole polarons can be produced in P3HT through the redox reaction between P3HT and $HAuCl_4$ (Equation S1), which changes its polarizability manifested by noticeable variations in the complex dielectric function (See Figure S4a). The modified refractive index dramatically shifts the interference condition, producing a new set of distinct

https://doi.org/10.1021/acsami.3c11940
ACS Appl. Mater. Interfaces 2023, 15, 51753−51762

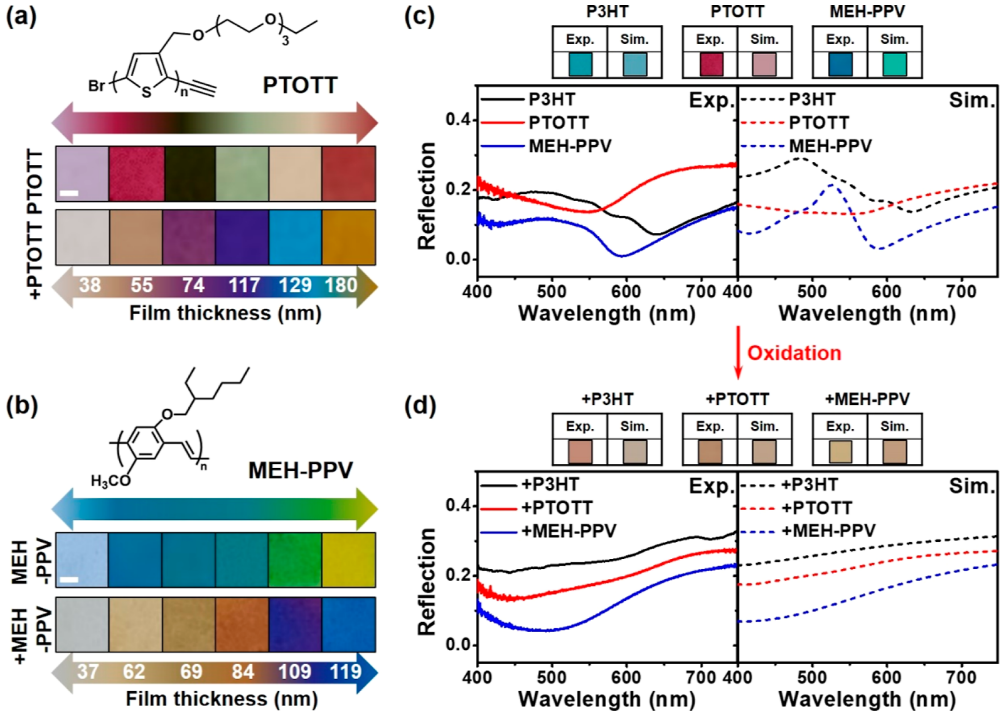

Figure 2. Thin-film interference color of other types of conjugated polymers. (a,b) Chemical structure and photograph of (a) PTOTT and (b) MEH-PPV with various thicknesses on a Si substrate (scale bar: 1 mm). (c,d) Experimental (left) and simulated (right) reflectance spectra and corresponding colors of (c) initial polymer and (d) oxidized polymer (oxidation condition: 500 μM $HAuCl_4$, 1 min) films of similar thickness (P3HT: 50, PTOTT: 55, and MEH-PPV: 62 nm) on Si. Calculations were performed with a transfer matrix algorithm, where the optical constants n and k for the conjugated polymers were measured by ellipsometry (Figure S4) and those for substrate materials were obtained from ellipsometry measurements and tabulated data (Figure S8).[33,34] Simulated thicknesses of 54, 60, and 57 nm for P3HT, PTOTT, and MEH-PPV, respectively, resulted in a good match between experimental and simulated colors.

thickness-dependent colors, as shown in Figure 1b (bottom). The color-changing process was monitored over time. Each row in Figure 1c is a photograph of 25, 85, and 125 nm thick P3HT films on silicon as a function of the oxidation time. A gradual color change was observed during oxidation of the 25 nm thick P3HT film from light blue to gray, whereas the 85 nm thick P3HT film shifted from green to purple and the 125 nm thick P3HT film shifted from yellow to blue. The gradated colors indicate that the thin-film interference color can be fine-tuned by adjusting the degree of polaron formation. In other words, color variation can be correlated to the extent of oxidation.

Redox of P3HT converts the real and imaginary parts of the complex refractive index, as shown in Figure S4a. Figure 1d presents the evolving reflection spectra for a 125 nm thick P3HT film on silicon due to the changing refractive index, where the peak position shifts from approximately 650 to 550 nm with intensity decrease. On the other hand, the absorption spectra in Figure 1e carried out with a P3HT film on a transparent glass substrate show intensity variations rather than spectral shifts. The index of glass is closer to that of the polymer film, which limits the reflection from the polymer–substrate interface in such a way that the film colors are dominated by absorption. As the oxidation reaction proceeds, the absorption at 520 nm assigned to the π–π^* transition of P3HT decreases in intensity, and a new absorption band appears at 800 nm, characteristic of the hole polaron state (Figure 1e). Previous studies have monitored the redox state of P3HT based on the changes in its absorbance.[6,20,29] In this approach, the color changes were mostly limited to intensity differences within a small range of colors, usually from red to a dimer or transparent state. However, when the P3HT film is on Si, the reflected color changes over a wider range of shades such as from yellow to blue, as shown in the time-dependent color photographs in the inset of Figure 1d. This highlights the merits of the thin-film interference where the mechanism provides visually clearer contrast between different redox states compared to colors based on absorption.

Extending to Other Types of the Conjugated Polymers. To assess the generality of our approach, we employed two additional conjugated polymers, poly[3-(2,5,8,11-tetraoxatridecanyl)thiophene] (PTOTT) and poly-[2-methoxy-5-(2-ethylhexyloxy)-1,4-phenylenevinylene] (MEH-PPV), for the fabrication of responsive color films. A thiophene derivative, PTOTT, shares the same polymer backbone as P3HT but has a different side chain, and thus, its packing, molar volume, and refractive index are different from those of P3HT. A widely studied conjugated polymer, MEH-PPV, was selected as a representative nonthiophene polymer. PTOTT was synthesized by a previously reported synthetic procedure[30−32] (characterization data in Figures S5 and S6), and commercial MEH-PPV was used as purchased. Optical and electrochemical characterization data for selected polymers are provided in Figures S7 and S2.

The PTOTT films on the Si substrates showed the interference colors evolving from purple to green to brown with a change in film thickness from 38 to 180 nm (Figure 2a, top). When oxidized by $HAuCl_4$, a new set of interference colors were observed, varying from gray to blue to yellow (Figure 2a, bottom). The MEH-PPV films also showed the

https://doi.org/10.1021/acsami.3c11940
ACS Appl. Mater. Interfaces 2023, 15, 51753−51762

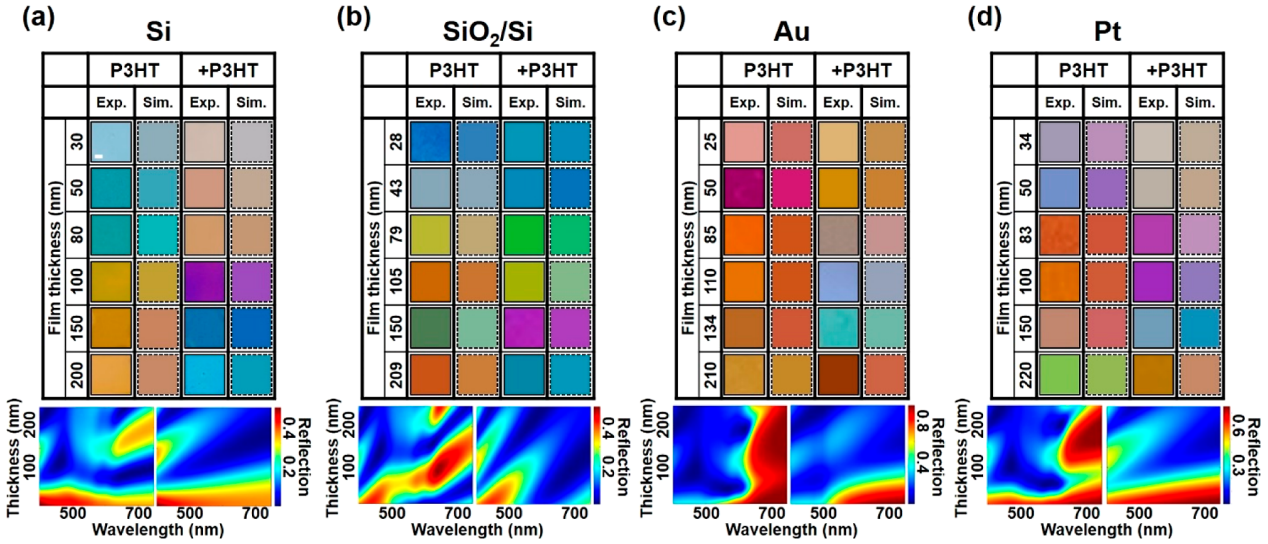

Figure 3. Thin-film interference colors for P3HT and +P3HT films on various substrates. Series of measured and calculated colors (top) and calculated reflection (bottom) as a function of film thickness and wavelength of P3HT and +P3HT films with different thicknesses on (a) Si, (b) SiO_2/Si, (c) Au/Si, and (d) Pt/Si substrates (scale bar: 3 mm).

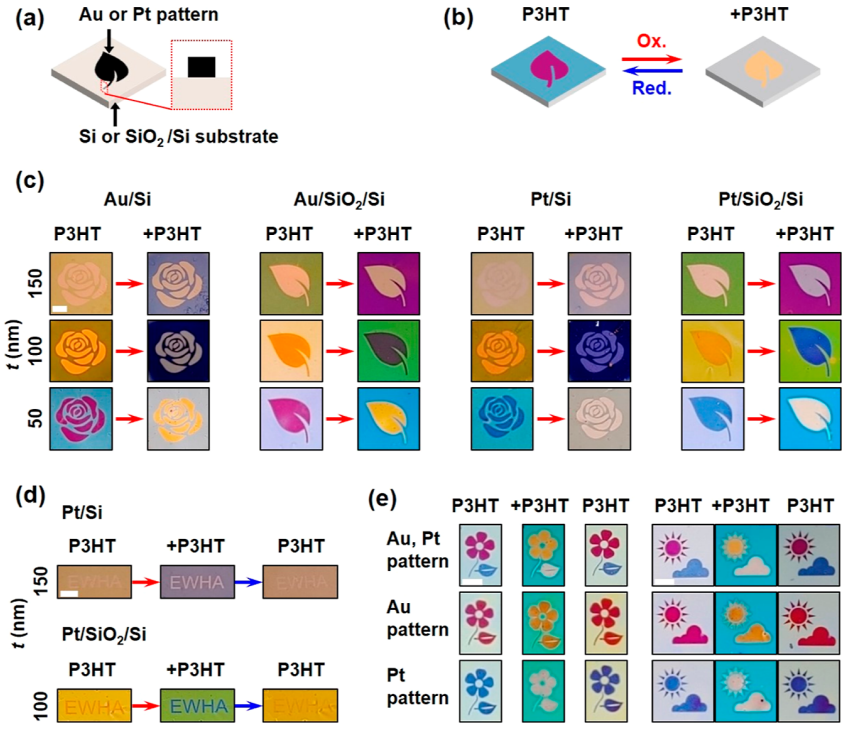

Figure 4. Thin-film interference colors from P3HT and +P3HT films on a metal-patterned substrate. (a) Schematic of the metal-patterned substrate consisting of Au or Pt metal patterns on Si substrate or 300 nm SiO_2 layer on Si substrate. (b) Schematic of the tunable structural color depending on the oxidation state of the polymer film on the metal-patterned substrate. (c) Photographs of the 150, 100, and 50 nm thick P3HT and +P3HT films on various types of the metal-patterned substrates. (d) Photographs of the EWHA logo during oxidation and reduction for decryption and encryption, respectively. (e) Photographs of P3HT, +P3HT, and reverted P3HT films on a dual metal pattern on SiO_2/Si substrates (top row) and single metal pattern on SiO_2/Si substrates (middle and bottom rows). For all experiments, P3HT oxidation was induced using a 500 μM aqueous solution of $HAuCl_4$, and the P3HT reduction was induced by exposure to pyrrole vapor (scale bar: 2 mm).

interference color changes depending on their thickness and oxidation state (Figure 2b). Due to their different refractive indices (see Figure S4, black), the three different polymer films (i.e., P3HT, PTOTT, MEH-PPV) at the neutral state showed distinct colors at the same thickness. For example, the 50−60 nm thick film of P3HT (50 nm), PTOTT (55 nm), and MEH-PPV (62 nm) exhibited greenish-blue, reddish-purple, and blue colors, respectively (Figure 2c, top). After oxidation, the refractive indices become similar (Figure S4, blue) such that the film colors were converted from their initial states to slightly toned brownish-grays, as shown in Figure 2d (top). These color transitions were investigated by electromagnetic

https://doi.org/10.1021/acsami.3c11940
ACS Appl. Mater. Interfaces 2023, 15, 51753−51762

field simulations, modeling the thin-film interference at the pristine and polaronic states. The calculations were performed through a transfer matrix method, where light was normally injected through air onto a polymer film on a substrate (see Supporting Information for the detailed simulation parameters). Figure 2c,d displays the experimental and simulated results for each film, respectively. In general, the experimental color and the reflectance spectra for P3HT (50 nm), PTOTT (55 nm), and MEH-PPV (62 nm) films match fairly well with those of the simulations, confirming that the thin-film interference is the colorant mechanism. The slight discrepancy in intensity and shade for the measured and simulated colors are attributed to two reasons. One is that the experimental images are raw photographs of the samples whose colors are weighted by the spectrum of the ambient light. The simulated colors, on the other hand, are free from the influence of the light source. The second reason is that the photographs were taken at slightly off-normal angles such that the optical path length of light traveling in the film is larger than that in the simulated film. These contribute to small shifts in the color depending on the wavelength, thickness, and refractive index.

Interestingly, the PTOTT and P3HT films of similar thicknesses showed distinct colors of reddish-purple and blue, respectively, despite sharing the same polymer backbone. On the other hand, similar colors were observed for the MEH-PPV and P3HT films. We also note that the thin-film interference colors of PTOTT and MEH-PPV are quite different, although their thin-film absorption spectra are similar (Figure S7). These results suggest that regardless of the chemical structure and the absorption property, MEH-PPV and P3HT share similar refractive indices, while PTOTT and P3HT do not. Given the current lack of research on photonic structural colors from the conjugated polymers, our simple approach can serve as the basis for evaluating the optical properties of polymers and their dynamic tunability.

Multicolor Films with the Patterned Substrates. Developing multicolor visual cues is important for reliable and rapid on-site visual diagnostics for colorimetric sensors. However, spatially modulating the thickness of a single polymer film in selective areas is a nontrivial task. Here, we exploit the metal-patterned substrates for a responsive multicolor system. A rigorous treatment of the reflection considers multiple reflections occurring between the top and bottom interfaces of the film, which are captured in the higher order reflection coefficients.[12,35] These terms are usually negligible, especially when the index contrast between film and surrounding is small. Otherwise, the total sum of the reflection coefficients determines the reflection, where the coefficients are defined by the complex refractive index of the substrate and film. Differences in the complex refractive index among substrates cause deviations in the phase shifts for the reflection coefficients, ultimately modifying the interference conditions and the corresponding colors.

Figure 3a–d presents the experimental and simulated colors along with calculated reflection spectra for P3HT and +P3HT supported by Si, SiO_2 (300 nm) on Si (SiO_2/Si), Au (100 nm) on Si (Au/Si), and Pt (100 nm) on Si (Pt/Si) substrates, respectively. Various thin-film interference colors were observed depending on the type of substrates as well as the film thickness and the oxidation state. For example, a purple color was observable for P3HT on gold and a clear blue for P3HT on SiO_2/Si, which were not seen on Si. These results indicate that the thin-film interference colors of P3HT and +P3HT films can be effectively modulated by the choice of the substrate.

Accordingly, we created multicolor films by adopting a metal-patterned Si or SiO_2/Si substrate (Figure 4). Au or Pt patterns were fabricated on Si or SiO_2/Si substrates through photolithography (Figure 4a). A single polymer layer of uniform thickness was then coated on the metal-patterned substrate, where the polymer thickness remained constant regardless of the underlying material (Figure S9). Distinct reflective colors were observed on the metal and the parts of the film (Figure 4b–c). The colors appearing on the metal-patterned substrates are consistent with those found on each respective material (Figure 3), confirming that the color contrasts are due to the reflective substrate rather than the polymer thickness. The distinct colors from the underlying patterns can undergo further changes with the oxidation state of P3HT, resulting in patterns with different shapes and background color combinations (Figure 4c,d). For example, purple rose in a blue background turns to yellow rose in a gray background with oxidation (the 50 nm thick P3HT film on the Au/Si substrate in Figure 4c). Again, different color sets can be readily obtained by varying the thickness of polymer films, as presented in Figure 4c. Among various color combinations, we point out two interesting color-changing behaviors. First, in the case of the 150 nm thick P3HT film on Au/Si or Pt/Si and the 100 nm thick P3HT on Pt/SiO_2/Si, the reflective colors from the substrate and the metal pattern are nearly indistinguishable in the pristine state but become clearly distinct after P3HT is oxidized as shown in Figure 4c. Such feature is useful for fabricating encryption–decryption devices. Figure 4d illustrates the effect revealing the letter "EWHA" with oxidation, which can be concealed again by exposing the oxidized polymer film to a reductive vapor, such as pyrrole (Figure 4d). Second, the 150 nm thick P3HT on Au/SiO_2/Si and Pt/SiO_2/Si shows clear oxidation-induced color changes on the background with negligible color changes on the leaf metal pattern. Such behavior is useful for smart labeling, where the static color can be used to monitor the stability of the sensor and the dynamic color can be used to monitor the environmental change.

The ability to add more colors expands the breadth of information that can be conveyed. Figure 4e presents a tricolor system from two metal patterns displaying three distinct colors on one substrate (top row), along with the single metal (Au or Pt) patterns (middle and bottom rows). P3HT on the Au (flower, sun) and Pt (leaf, cloud) patterns appeared purple and blue, which shifted to yellow and white after oxidation, respectively. All observed color changes were reversible, as shown in Figure 4e. It is also interesting to note that the boundary of the pattern is sharp in the P3HT film but becomes blurry after the P3HT film is oxidized (Figure 4e). This effect is clearly seen in the line profile across the boundaries of the sun ray pattern, showing abrupt and gradual color transitions at the pattern boundaries for the oxidized and pristine P3HT films, respectively (Figure S10). This is because the thickness-dependent behavior varies with the polymer oxidation state and the substrate type. This feature was also reversible with chemical reduction (Figure 4e). These results illustrate that the combination of polymer thickness and substrate type provides high degrees of freedom for managing colors and their transitions.

Effect of Oxidants on the Color Responsivity. The responsivity of +P3HT thin-film color to reductive vapors can

https://doi.org/10.1021/acsami.3c11940
ACS Appl. Mater. Interfaces 2023, 15, 51753–51762

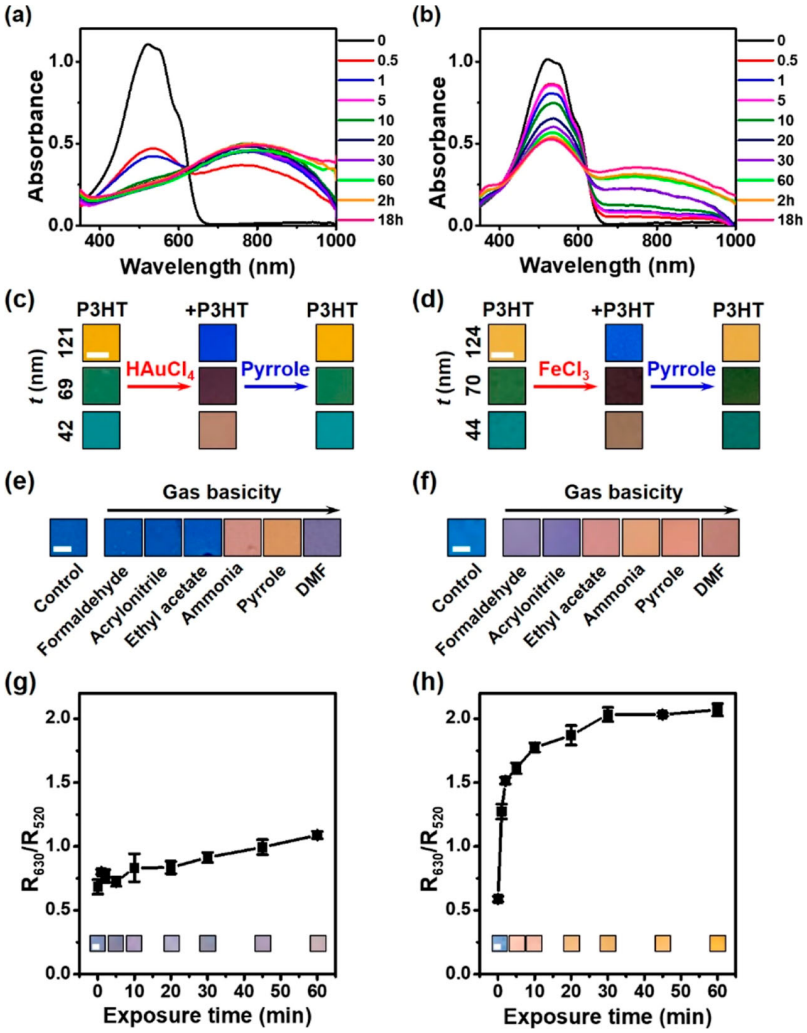

Figure 5. Characteristics of the +P3HT films prepared by different oxidizing agents. (a,b) Time-dependent UV−vis spectra of the P3HT film oxidized by dipping in aqueous solutions of (a) 500 μM $HAuCl_4$ and (b) 500 μM $FeCl_3$. Each subsequent scan occurred at 0, 0.5, 1, 5, 10, 20, 30, 60 min, 2 h, and 18 h. (c,d) Photographs of the original 125 nm thick P3HT film (yellow color, top), the 70 nm thick P3HT film (green color, middle), and the 40 nm-thick P3HT film (sky blue color, bottom), after oxidation by dipping in (c) a 500 μM aqueous solution of $HAuCl_4$ for 30 s or (d) a 10 mM acetonitrile solution of $FeCl_3$ for 1 min and after reduction by exposure to pyrrole vapor. (e,f) Photographs of the 125 nm thick +P3HT films prepared by dipping in (e) a 500 μM $HAuCl_4$ solution for 30 s or (f) a 10 mM $FeCl_3$ solution for 1 min before and after exposures to various chemical vapor environments. (g,h) Time-dependent ratio of reflection (R_{630}/R_{520}) of the 110 nm thick +P3HT films prepared by dipping in (g) a 500 μM $HAuCl_4$ solution for 30 s or (h) a 10 mM $FeCl_3$ solution for 1 min exposed to DMF vapor. The insets show photographs of the +P3HT films exposed to DMF over time. (c−f) Scale bars: 1 mm. (g,h) The length of one side of the inset picture is 2 mm.

vary with the nature and degree of oxidation, which can be controlled by the type of oxidants, as well as the oxidation time and the oxidant concentration. To investigate the effects of oxidizing agents to the color responsivity, the P3HT films were treated with a common oxidizing agent, $FeCl_3$ (Equation S2), as well as $HAuCl_4$. Figure 5a,b presents the extinction spectra measured over time during oxidation by aqueous solutions $HAuCl_4$ and $FeCl_3$, respectively, both of which show increases of the hole polaron band at 800 nm but at different rates. $HAuCl_4$ is a stronger oxidizing agent than $FeCl_3$ with the reduction potential of +1.5 V and +0.77 V,[36] respectively (Figure S3), which explains the faster reaction rate with $HAuCl_4$. Exposure of the P3HT films to metal complexes with a lower reduction potential such as $CuCl_2$ does not cause any color change as expected (reaction 3 in Figures S3, S11c). For $FeCl_3$, the oxidation of P3HT is accompanied by the reduction of $FeCl_3$ to $FeCl_2$ (reaction 1 in Figures S3, S12a).[37] For $HAuCl_4$, the oxidation occurs with the reduction of $HAuCl_4$ to Au nanoparticles (reaction 2 in Figures S3, S12b,c).

Nonetheless, the same set of thickness-dependent and doping-induced colors could be generated with $FeCl_3$ and $HAuCl_4$ by adjusting the oxidation condition (i.e., oxidant concentration and oxidation time, Figure 5a,b). Likewise, both +P3HT films showed color responsivity to reductive vapors, as demonstrated with pyrrole (Figure 5c,d). However, the responsivity of +P3HT to reductive vapors varied significantly, depending on the type of oxidant used to generate the hole polarons (Figure 5e,h). Figure 5e,f presents the photographs of +P3HT films oxidized by $HAuCl_4$ and $FeCl_3$, respectively, before and after exposure to *N*,*N*-dimethylformamide (DMF), pyrrole, ammonia, ethyl acetate, acrylonitrile, and formaldehyde vapor for 1 h in a closed system (Figure S13). The +P3HT film oxidized by $FeCl_3$ exhibited a color shift from blue to yellow contingent on the reducing power of the exposed

https://doi.org/10.1021/acsami.3c11940
ACS Appl. Mater. Interfaces 2023, 15, 51753−51762

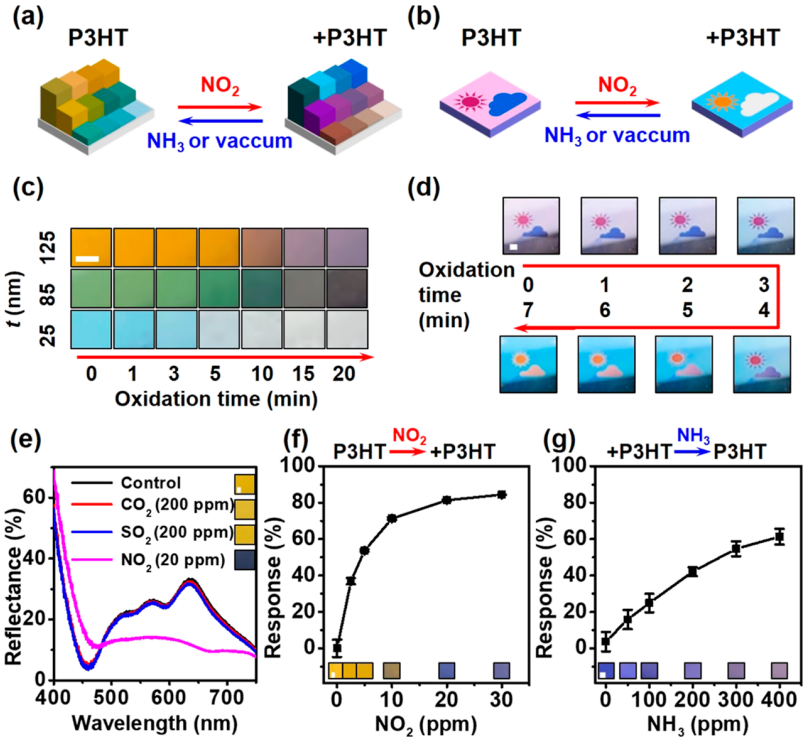

Figure 6. Multicolor responses of the P3HT and +P3HT films to oxidative or reductive vapors. (a,b) Schematic of the responsive multicolor gas sensor using the P3HT films (a) with different thicknesses and (b) on a metal-patterned substrate. (c) Photographs of the 125 nm thick P3HT (top), the 85 nm thick P3HT film (middle), and the 25 nm thick P3HT film (bottom) exposed to 50 ppm of NO_2 gas flow [1000 standard cubic centimeters per minute (SCCM)] over time. (d) Photographs of the P3HT film coated on a dual metal-patterned substrate (sun pattern: Au, cloud pattern: Pt, substrate: SiO_2/Si) during oxidation by using 100 ppm of NO_2 gas flow (1000 SCCM) over time. (e) Reflectance spectra and color change of the P3HT film upon exposure to oxidative gases (gas calculated as the relative change of reflection ratio at 630 and 460 nm) (Response (%) = $\Delta R_{630}/R_{460}$ response ÷ R_{630}/R_{460} initial ×100) for NO_2 sensing and 475 and 610 nm (Response (%) = $\Delta R_{630}/R_{460}$ response ÷ R_{475}/R_{610} initial ×100) for NH_3 sensing. (c,d) Scale bars: 1 mm. (e–g) The length of one side of the inset picture: 4 mm.

chemical vapor. Specifically, the blue +P3HT films exposed to formaldehyde (683.3 kJ/mol)[38] and acrylonitrile (753.7 kJ/mol)[38] with relatively a low gas-phase basicity turned to purple, and the +P3HT films exposed to ethyl acetate (804.7 kJ/mol),[38] ammonia (819.0 kJ/mol),[38] pyrrole (843.8 kJ/mol),[38] and DMF (856.6 kJ/mol)[38] with relatively a high basicity showed a greater degree of color change to yellow. When oxidized by $HAuCl_4$, the +P3HT films were found to only react to vapors with a higher basicity threshold that excludes ethyl acetate, acrylonitrile, and formaldehyde under the reaction condition. In addition, the +P3HT film prepared with $HAuCl_4$ showed less reactivity to DMF than pyrrole and ammonia despite its higher basicity because it has a lower vapor pressure than other tested solvents. On the other hand, the +P3HT film prepared with $FeCl_3$ showed a high responsivity even to the low vapor pressure DMF. The reactivity of the +P3HT film was further monitored by taking reflection spectra over time during the reduction process with DMF. The responsivity was quantified by taking the ratio between the reflection intensity at 630 nm (R_{630}), reflection peak position of the pristine film, and the reflection intensity at 520 nm (R_{520}), π–π^* absorption peak position of the pristine film (original reflectance data shown in Figure S14). As can be seen from the reflection ratio plot and the film color in the inset (Figure 5), the +P3HT film prepared with $HAuCl_4$ (Figure 5g) exhibited a slower response rate and a less reactivity to DMF vapor than the film prepared with $FeCl_3$ (Figure 5h).

Fourier transform-infrared analysis showed characteristic intensity reduction of IR bands with hole doping,[39−41] which were almost fully recovered upon exposure to pyrrole (Figure S15). In addition, IR bands corresponding to irreversible oxidation products such as sulfoxides, sulfones or sulfonic acids,[42] unsaturated hydroperoxides, or carboxylic acid derivatives[43] were not found in both cases. These results indicate that the chemical integrity of the film is maintained after a redox cycle for both oxidants. The dedoping process of the $HAuCl_4$-treated P3HT films has been explained by the reduction of $AuCl_4^-$ complexed with the thiophene ring of +P3HT through the strong sulfur–gold bond.[29] We attributed the lower responsivity of the $HAuCl_4$-treated films to the stronger interaction of +P3HT with $AuCl_4^-$,[44,45] which requires stronger reducing agents for dedoping. Taken together, these results demonstrate that the oxidation method of the P3HT film determines the nature of the oxidized film, which in turn affects the response time and sensitivity of +P3HT films to reductive vapor.

Multicolor Responses to Gaseous Species. The ability of the color-changing behavior to recognize harmful gases was further investigated for the NMR bands of NO_2 and NH_3. Our study proposes two strategies for the development of multicolor sensors, using the thickness (Figure 6a) and the substrate type (Figure 6b). Figure 6c shows the results of the NO_2 detection using the P3HT films with different thicknesses. NO_2 is an oxidizing gas that can generate holes in organic semiconductors. The as-prepared P3HT films show color

https://doi.org/10.1021/acsami.3c11940
ACS Appl. Mater. Interfaces 2023, 15, 51753−51762

changes in response to exposure to NO_2 due to the hole polaron generation in the P3HT film. The multicolor capability was enabled by the thickness-dependent concentration of CO_2 and SO_2: 200 ppm and NO_2: 20 ppm. (f,g) The time-dependent responses of (f) the 125 nm thick P3HT film exposed to various concentrations of the NO_2 gas and (g) +P3HT film prepared using $FeCl_3$ solution (10 mM in acetonitrile, 10 s exposure) exposed to the NH_3 gas. The insets show photographs of the P3HT and +P3HT films exposed to each gas. The gas response and color improve the reliability of the detection. The gas-sensing ability was also tested on our multicolor pattern made from a P3HT film on a dual metal-patterned substrate as shown in Figure 6d. The time-varying response of this film can be observed in Movie 1. When exposed to 100 ppm of NO_2 gas, the film showed color changes in the pattern and the background was consistent with that found under oxidizing solutions of $HAuCl_4$ and $FeCl_3$ within 3−5 min. The sensing selectivity was evaluated with 20 ppm of NO_2, 200 ppm of CO_2, and 200 ppm of SO_2. As shown in Figure 6e, significant changes in the reflectance spectra and structural color were observed only for NO_2 among the tested analytes even at concentrations that were 10 times lower than other tested gases, confirming the selectivity toward the NO_2 gas. Figure 6f presents the response of the P3HT films depending on the NO_2 concentration, which showed that the colorimetric responses increase with the concentration of NO_2 with significant changes in the reflection spectra at the lowest concentration of 2.5 ppm (original reflectance data in Figure S16). In Figure 6g, the +P3HT film oxidized by $FeCl_3$ was used for the detection of a reductive gas, NH_3, at varying concentrations, which showed the colorimetric responses down to 50 ppm (original reflectance data shown in Figure S17). The sensitivity allows for detection at or below the permissible exposure limits set by the National Institute for Occupational Safety and Health, which are 3 and 50 ppm for 8 h for NO_2 and NH_3, respectively.[46−48]

When the colorimetric film oxidized by the NO_2 gas was left in ambient air, vacuum, or the NH_3 gas environment, the color reverted back to its initial neutral state with the reversibility slightly degrading with multiple cycles (Figure S18). The reversibility may allow for reuse of the colored film, but the P3HT film is reasonably cost-effective even without reusability, as the colorimetric information can be visually assessed without any optical or electrical equipment. The mechanism of the P3HT reactivity to oxidative and reductive gases was explored previously in the context of organic field-effect transistor devices, where the carrier generation by doping increases the current.[49] Our method relies on changes in optical properties with doping/dedoping processes. Although the lower bounds to the sensitivity of our method are modest compared to electrical devices,[50−53] the colorimetric method reported here provides readily detectable visual signal without complicated devices and can be coupled with electrical devices when desired.

CONCLUSIONS

Multidimensional responsive colors were achieved with a conjugated polymer film on a reflective substrate through the simple thin-film interference mechanism. The polymer film exhibited a wide range of colors controllable with the film thickness and substrate type, which can be further shifted in response to the exposure to an oxidative or reductive environment through the generation or reduction of hole polarons in the polymer film. This mechanism was generally applicable to conventional conjugated polymers, such as P3HT, PTOTT, and MEH-PPV, demonstrating that the color combinations can be further expanded by the choice of conjugated polymers. The responsivity of the oxidized polymer films to a reductive environment can be modulated by the nature of oxidation. The polymer films oxidized with $FeCl_3$ showed a higher sensitivity and a shorter reaction time than the films prepared with a stronger oxidant, $HAuCl_4$, making them more suitable for the sensor applications. Nonetheless, $HAuCl_4$ can be conveniently used to prepare the oxidized polymer films due to its fast oxidation rate. Dual or tricolor devices were realized from a single polymer film by adopting the metal-patterned substrates to spatially modulate the thin-film interference. Such multicolor capability is a desirable attribute for various applications, including sensing, encryption, and smart display. Our conjugated polymer films therefore provide a facile, economical, yet robust approach to the design and fabrication of dynamic multicolor palettes.

EXPERIMENTAL SECTION

Preparation of the Conjugated Polymer Films. The P3HT (10−50 g/L) and MEH-PPV (4.5 g/L) solutions were prepared by dissolving them in 1,2-dichlorobenzene. The PTOTT (10−40 g/L) solution was prepared by dissolving it in a 9:1 mixture of acetonitrile and ethanol, heating the solution at 60 °C for 1 min, and vortexing it for 10 min at room temperature. The P3HT and PTOTT solutions were filtered by using a 0.2 μm PTFE filter before use. Silicon wafers were cleaned with piranha solution and prefunctionalized with hexamethyldisilazane, following a literature procedure.[54,55] The conjugated polymer solutions were spin-coated on silicon wafers at 1000−6000 rpm for 60 s. The polymer film thickness was controlled by changing the polymer concentration and spin-coating speed (Table S1) and measured by atomic force microscopy (Figure S1, Table S2). The oxidized P3HT films were prepared by dipping the spin-coated film into an aqueous or acetonitrile solution of $HAuCl_4$ or $FeCl_3$ (0.1−10 mM). The oxidized films were washed with water or acetonitrile and dried with N_2 to remove any residual dopant solution.

Fabrication of the Reflective Substrates. The metal-coated Si or SiO_2/Si substrates were prepared by using an ultrahigh vacuum direct current magnetron sputtering system with Cr (20 nm) and Ti (20 nm) as an adhesion layer for Pt (100 nm) and Au (100 nm), respectively. After deposition, the metal patterns were fabricated by UV photolithography. SiO_2/Si was prepared by thermal oxidation of the Si wafer.

Response of the P3HT Films to Reductive Organic Vapor. In a typical measurement, a polaronic P3HT film on a Si wafer was placed in a sealed vessel (4.5 cm diameter) with an aliquot of the selected liquid (100 μL) for 60 min until the chemical vapor reached its equilibrium pressure (Figure S13). Ammonium hydroxide solution (25%) was used to generate ammonia gas. All other vapors were generated from the corresponding pure liquid. Freshly prepared +P3HT films were used for all experiments, as they show discoloration to their original color states over time (Figure S19).

Response of the P3HT Films to Oxidative and Reductive Gases. The recognitions of P3HT for NO_2 and +P3HT for NH_3 were tested with a customized sensing measurement system. The P3HT or +P3HT films on a Si substrate were placed in a chamber with a quartz window. The inner volume of the chamber was approximately 100 cm^3, and the distance between the window and the sample stage was 6.5 mm. Selected gas was flowed into the chamber through a gas inlet and outlet, and the gas concentration was controlled by mass flow controllers. Photographs and reflectance spectra were obtained through the quartz window. Diffuse reflectance spectra were measured with an Ocean Optics Flame instrument equipped with an Ocean Optics HL-2000-LL halogen-deuterium light source and a 400 μm reflection probe.

https://doi.org/10.1021/acsami.3c11940
ACS Appl. Mater. Interfaces 2023, 15, 51753−51762

■ ASSOCIATED CONTENT

Supporting Information

The Supporting Information is available free of charge at https://pubs.acs.org/doi/10.1021/acsami.3c11940.

Detailed characterization data for the P3HT, PTOTT, and MEH-PPV films (i.e., TEM, AFM, ellipsometry, and reflectance spectra), detailed simulation procedures, diagram of reduction potentials, reaction equations, and a movie showing the color change of the P3HT film exposed to the NO_2 gas (PDF)

Movie 1 (MP4)

■ AUTHOR INFORMATION

Corresponding Authors

So-Jung Park − *Department of Chemistry and Nanoscience, Ewha Womans University, Seodaemun-gu, Seoul 03760, Republic of Korea;* orcid.org/0000-0002-6364-3754; Email: sojungpark@ewha.ac.kr

Jerome Kartham Hyun − *Department of Chemistry and Nanoscience, Ewha Womans University, Seodaemun-gu, Seoul 03760, Republic of Korea;* orcid.org/0000-0002-2630-5051

Wooyoung Lee − *Department of Materials Science and Engineering, Yonsei University, Seodaemun-gu, Seoul 03722, Korea;* orcid.org/0000-0001-8406-4324

Authors

Ji-eun Park − *Department of Chemistry and Nanoscience, Ewha Womans University, Seodaemun-gu, Seoul 03760, Republic of Korea*

Soomin Lee − *Department of Materials Science and Engineering, Yonsei University, Seodaemun-gu, Seoul 03722, Korea*

Youngji Kim − *Department of Chemistry and Nanoscience, Ewha Womans University, Seodaemun-gu, Seoul 03760, Republic of Korea*

Shine K. Albert − *Department of Chemistry and Nanoscience, Ewha Womans University, Seodaemun-gu, Seoul 03760, Republic of Korea*

Yumin Lee − *Department of Chemistry and Nanoscience, Ewha Womans University, Seodaemun-gu, Seoul 03760, Republic of Korea*

Complete contact information is available at: https://pubs.acs.org/10.1021/acsami.3c11940

Author Contributions

J. P. and S. L. contributed equally. The manuscript was written through contributions of all authors. All authors have given approval to the final version of the manuscript.

Notes

The authors declare no competing financial interest.

■ ACKNOWLEDGMENTS

This work was supported by the National Research Foundation of Korea (NRF) grant funded by the Korean government (MSIT) [NRF-2017R1A5A1015365 (S.-J. P., J. K. H.), RS-2023-00274736 (S.-J. P.), NRF-2019R1A6A1A11055660 (W. L.), NRF-2019R1C1C1002802 (J. K. H.), RS-2023-00239133 (J.-e. P.), NRF-2020M3D1A1110522 (J. K. H.)]. The work was also supported by the Technology Innovation Program (Program no. 20013621, Center for Super Critical Material Industrial Technology) funded by the Ministry of Trade, Industry & Energy (MOTIE, Korea) (W. L.) and the RP-Grant 2020 of Ewha Womans University (J.-e. P.).

■ REFERENCES

(1) Teyssier, J.; Saenko, S. V.; van der Marel, D.; Milinkovitch, M. C. Photonic Crystals cause Active Colour Change in Chameleons. *Nat. Commun.* **2015**, *6* (1), 6368.

(2) Phan, L.; Kautz, R.; Leung, E. M.; Naughton, K. L.; Van Dyke, Y.; Gorodetsky, A. A. Dynamic Materials Inspired by Cephalopods. *Chem. Mater.* **2016**, *28* (19), 6804−6816.

(3) Isapour, G.; Lattuada, M. Bioinspired Stimuli-Responsive Color-Changing Systems. *Adv. Mater.* **2018**, *30* (19), 1707069.

(4) Kinoshita, S.; Yoshioka, S. Structural Colors in Nature: The Role of Regularity and Irregularity in the Structure. *ChemPhysChem* **2005**, *6* (8), 1442−1459.

(5) Aleisa, R.; Feng, J.; Ye, Z.; Yin, Y. Rapid High-Contrast Photoreversible Coloration of Surface-Functionalized N-Doped TiO_2 Nanocrystals for Rewritable Light-Printing. *Angew. Chem., Int. Ed.* **2022**, *61* (28), No. e202203700.

(6) Chou, H.-H.; Nguyen, A.; Chortos, A.; To, J. W. F.; Lu, C.; Mei, J.; Kurosawa, T.; Bae, W.-G.; Tok, J. B. H.; Bao, Z. A chameleon-inspired stretchable electronic skin with interactive colour changing controlled by tactile sensing. *Nat. Commun.* **2015**, *6* (1), 8011.

(7) Duan, X.; Kamin, S.; Liu, N. Dynamic plasmonic colour display. *Nat. Commun.* **2017**, *8* (1), 14606.

(8) Lin, H.; Song, L.; Huang, Y.; Cheng, Q.; Yang, Y.; Guo, Z.; Su, F.; Chen, T. Macroscopic Au@PANI Core/Shell Nanoparticle Superlattice Monolayer Film with Dual-Responsive Plasmonic Switches. *ACS Appl. Mater. Interfaces* **2020**, *12* (9), 11296−11304.

(9) Li, J.; Chen, Y.; Hu, Y.; Duan, H.; Liu, N. Magnesium-Based Metasurfaces for Dual-Function Switching between Dynamic Holography and Dynamic Color Display. *ACS Nano* **2020**, *14* (7), 7892−7898.

(10) Qin, M.; Sun, M.; Bai, R.; Mao, Y.; Qian, X.; Sikka, D.; Zhao, Y.; Qi, H. J.; Suo, Z.; He, X. Bioinspired Hydrogel Interferometer for Adaptive Coloration and Chemical Sensing. *Adv. Mater.* **2018**, *30* (21), 1800468.

(11) Song, H. S.; Lee, G. J.; Yoo, D. E.; Kim, Y. J.; Yoo, Y. J.; Lee, D.-W.; Siva, V.; Kang, I.-S.; Song, Y. M. Reflective color filter with precise control of the color coordinate achieved by stacking silicon nanowire arrays onto ultrathin optical coatings. *Sci. Rep.* **2019**, *9* (1), 3350.

(12) Lee, Y.; Yun, J.; Seo, M.; Kim, S.-J.; Oh, J.; Kang, C. M.; Sun, H.-J.; Chung, T. D.; Lee, B. Full-Color-Tunable Nanophotonic Device Using Electrochromic Tungsten Trioxide Thin Film. *Nano Lett.* **2020**, *20* (8), 6084−6090.

(13) Argun, A. A.; Aubert, P.-H.; Thompson, B. C.; Schwendeman, I.; Gaupp, C. L.; Hwang, J.; Pinto, N. J.; Tanner, D. B.; MacDiarmid, A. G.; Reynolds, J. R. Multicolored Electrochromism in Polymers: Structures and Devices. *Chem. Mater.* **2004**, *16* (23), 4401−4412.

(14) Grimsdale, A. C.; Leok Chan, K.; Martin, R. E.; Jokisz, P. G.; Holmes, A. B. Synthesis of light-emitting conjugated polymers for applications in electroluminescent devices. *Chem. Rev.* **2009**, *109* (3), 897−1091.

(15) Zhang, D.; Qiao, J.; Zhang, D.; Duan, L. Ultrahigh-Efficiency Green PHOLEDs with a Voltage under 3 V and a Power Efficiency of Nearly 110 lm W^{-1} at Luminance of 10 000 cd m^{-2}. *Adv. Mater.* **2017**, *29* (40), 1702847.

(16) Yang, Y.; Zhang, Z.-G.; Bin, H.; Chen, S.; Gao, L.; Xue, L.; Yang, C.; Li, Y. Side-Chain Isomerization on an n-type Organic Semiconductor ITIC Acceptor Makes 11.77% High Efficiency Polymer Solar Cells. *J. Am. Chem. Soc.* **2016**, *138* (45), 15011−15018.

(17) Oh, J. Y.; Rondeau-Gagné, S.; Chiu, Y.-C.; Chortos, A.; Lissel, F.; Wang, G.-J. N.; Schroeder, B. C.; Kurosawa, T.; Lopez, J.; Katsumata, T.; et al. Intrinsically stretchable and healable semiconducting polymer for organic transistors. *Nature* **2016**, *539* (7629), 411−415.

(18) Vegiraju, S.; He, G.-Y.; Kim, C.; Priyanka, P.; Chiu, Y.-J.; Liu, C.-W.; Huang, C.-Y.; Ni, J.-S.; Wu, Y.-W.; Chen, Z.; et al. Solution-Processable Dithienothiophenoquinoid (DTTQ) Structures for Ambient-Stable n-Channel Organic Field Effect Transistors. *Adv. Funct. Mater.* **2017**, *27* (21), 1606761.
(19) Beaujuge, P. M.; Reynolds, J. R. Color Control in π-Conjugated Organic Polymers for Use in Electrochromic Devices. *Chem. Rev.* **2010**, *110* (1), 268−320.
(20) Kim, J.; Rémond, M.; Kim, D.; Jang, H.; Kim, E. Electrochromic Conjugated Polymers for Multifunctional Smart Windows with Integrative Functionalities. *Adv. Mater. Technol.* **2020**, *5* (6), 1900890.
(21) Huang, W. S.; MacDiarmid, A. G. Optical properties of polyaniline. *Polymer* **1993**, *34* (9), 1833−1845.
(22) Dane, E. L.; King, S. B.; Swager, T. M. Conjugated Polymers That Respond to Oxidation with Increased Emission. *J. Am. Chem. Soc.* **2010**, *132* (22), 7758−7768.
(23) Cativo, M. H. M.; Kamps, A. C.; Gao, J.; Grey, J. K.; Hutchison, G. R.; Park, S.-J. Oxidation-Induced Photoluminescence of Conjugated Polymers. *J. Phys. Chem. B* **2013**, *117* (16), 4528−4535.
(24) Moon, C. W.; Park, J.-e.; Park, M.; Kim, Y.; Narasimha, K.; Hyun, J. K.; Park, S.-J. Responsive Thin-Film Interference Colors from Polaronic Conjugated Block Copolymers. *ACS Appl. Mater. Interfaces* **2021**, *13* (1), 1555−1561.
(25) Lanfranchi, A.; Megahd, H.; Lova, P.; Comoretto, D. Multilayer Polymer Photonic Aegises Against Near-Infrared Solar Irradiation Heating. *ACS Appl. Mater. Interfaces* **2022**, *14* (12), 14550−14560.
(26) Al-Ibrahim, M.; Roth, H. K.; Schroedner, M.; Konkin, A.; Zhokhavets, U.; Gobsch, G.; Scharff, P.; Sensfuss, S. The influence of the optoelectronic properties of poly(3-alkylthiophenes) on the device parameters in flexible polymer solar cells. *Org. Electron.* **2005**, *6* (2), 65−77.
(27) Heeney, M.; Zhang, W.; Crouch, D. J.; Chabinyc, M. L.; Gordeyev, S.; Hamilton, R.; Higgins, S. J.; McCulloch, I.; Skabara, P. J.; Sparrowe, D.; et al. Regioregular poly(3-hexyl)selenophene: a low band gap organic hole transporting polymer. *Chem. Commun.* **2007**, No. 47, 5061−5063.
(28) Acevedo-Peña, P.; Baray-Calderón, A.; Hu, H.; González, I.; Ugalde-Saldivar, V. M. Measurements of HOMO-LUMO levels of poly(3-hexylthiophene) thin films by a simple electrochemical method. *J. Solid State Electrochem.* **2017**, *21* (8), 2407−2414.
(29) Zhao, D.; Li, L.; Niu, W.; Chen, S. Highly conductive polythiophene films doped with chloroauric acid for dual-mode sensing of volatile organic amines and thiols. *Sens. Actuators, B* **2017**, *243*, 380−387.
(30) Sheina, E. E.; Khersonsky, S. M.; Jones, E. G.; McCullough, R. D. Highly Conductive, Regioregular Alkoxy-Functionalized Polythiophenes: A New Class of Stable, Low Band Gap Materials. *Chem. Mater.* **2005**, *17* (13), 3317−3319.
(31) Kamps, A. C.; Cativo, M. H. M.; Fryd, M.; Park, S.-J. Self-Assembly of Amphiphilic Conjugated Diblock Copolymers into One-Dimensional Nanoribbons. *Macromolecules* **2014**, *47* (1), 161−164.
(32) Kamps, A. C.; Cativo, M. H. M.; Chen, X.-J.; Park, S.-J. Self-Assembly of DNA-Coupled Semiconducting Block Copolymers. *Macromolecules* **2014**, *47* (11), 3720−3726.
(33) Palik, E.; Edward, D. P. *Handbook of Optical Constants of Solids*; Academic Press, 1998; Vol. *3*.
(34) Johnson, P. B.; Christy, R. W. Optical Constants of the Noble Metals. *Phys. Rev. B* **1972**, *6* (12), 4370−4379.
(35) Wang, Z.; Wang, X.; Cong, S.; Chen, J.; Sun, H.; Chen, Z.; Song, G.; Geng, F.; Chen, Q.; Zhao, Z. Towards full-colour tunability of inorganic electrochromic devices using ultracompact fabry-perot nanocavities. *Nat. Commun.* **2020**, *11* (1), 302.
(36) Haynes, W. M.; Lide, R. D.; Bruno, J. T. *CRC Handbook of Chemistry and Physics*; CRC Press, 2005.
(37) Kang, Y. H.; Ko, S.-J.; Lee, M.-H.; Lee, Y. K.; Kim, B. J.; Cho, S. Y. Highly efficient and air stable thermoelectric devices of poly(3-hexylthiophene) by dual doping of Au metal precursors. *Nano Energy* **2021**, *82*, 105681.
(38) Hunter, E. P. L.; Lias, S. G. Evaluated Gas Phase Basicities and Proton Affinities of Molecules: An Update. *J. Phys. Chem. Ref. Data* **1998**, *27* (3), 413−656.
(39) Yamamoto, J.; Furukawa, Y. Electronic and Vibrational Spectra of Positive Polarons and Bipolarons in Regioregular Poly(3-hexylthiophene) Doped with Ferric Chloride. *J. Phys. Chem. B* **2015**, *119* (13), 4788−4794.
(40) Singh, R. K.; Kumar, J.; Singh, R.; Kant, R.; Rastogi, R. C.; Chand, S.; Kumar, V. Structure-conductivity correlation in ferric chloride-doped poly(3-hexylthiophene). *New J. Phys.* **2006**, *8* (7), 112.
(41) Hegelund, F.; Wugt Larsen, R.; Palmer, M. H. The high-resolution infrared spectrum of thiophene between 600 and 1200 cm-1: A spectroscopic and theoretical study of the fundamental bands ν6, ν7, ν13, and the c-Coriolis interacting dyad ν5, ν19. *J. Mol. Spectrosc.* **2008**, *247* (1), 100−114.
(42) Sai, N.; Leung, K.; Zádor, J.; Henkelman, G. First principles study of photo-oxidation degradation mechanisms in P3HT for organic solar cells. *Phys. Chem. Chem. Phys.* **2014**, *16* (17), 8092−8099.
(43) González-Juárez, E.; García-Hernández, E.; Arrieta-González, C. D.; Salgado-Delgado, R.; Güizado-Rodríguez, M.; Barba, V.; Espinosa-Roa, A. P3HT colloid stability study and its application in the degradation of methylene blue dye under UV radiation conditions. *Polym. Bull.* **2021**, *78* (11), 6455−6472.
(44) Storhoff, J. J.; Elghanian, R.; Mucic, R. C.; Mirkin, C. A.; Letsinger, R. L. One-Pot Colorimetric Differentiation of Polynucleotides with Single Base Imperfections Using Gold Nanoparticle Probes. *J. Am. Chem. Soc.* **1998**, *120* (9), 1959−1964.
(45) Dishner, M. H.; Hemminger, J. C.; Feher, F. J. Formation of a Self-Assembled Monolayer by Adsorption of Thiophene on Au(111) and Its Photooxidation. *Langmuir* **1996**, *12* (26), 6176−6178.
(46) Leung, C. M.; Foo, C. L. Mass ammonia inhalational burns-experience in the management of 12 patients. *Ann. Acad. Med. Singapore* **1992**, *21* (5), 624−629.
(47) Kim, D.-H.; Cha, J.-H.; Lim, J. Y.; Bae, J.; Lee, W.; Yoon, K. R.; Kim, C.; Jang, J.-S.; Hwang, W.; Kim, I.-D. Colorimetric Dye-Loaded Nanofiber Yarn: Eye-Readable and Weavable Gas Sensing Platform. *ACS Nano* **2020**, *14* (12), 16907−16918.
(48) Methner, M. M.; Delaney, L. J.; Tubbs, R. L. *Air Contaminant and Noise Exposures Among Transportation Security Administration (TSA) Baggage Screeners at Four International Airports*; National Institute for Occupational Safety and Health, 2005.
(49) Xie, T.; Xie, G.; Du, H.; Zhou, Y.; Xie, F.; Jiang, Y.; Tai, H. The Fabrication and Optimization of Thin-Film Transistors Based on Poly(3-Hexylthiophene) Films for Nitrogen Dioxide Detection. *IEEE Sens. J.* **2016**, *16* (7), 1865−1871.
(50) Bielecki, Z.; Stacewicz, T.; Smulko, J.; Wojtas, J. Ammonia Gas Sensors: Comparison of Solid-State and Optical Methods. *Appl. Sci.* **2020**, *10* (15), 5111.
(51) Farea, M. A.; Mohammed, H. Y.; Shirsat, S. M.; Sayyad, P. W.; Ingle, N. N.; Al-Gahouari, T.; Mahadik, M. M.; Bodkhe, G. A.; Shirsat, M. D. Hazardous gases sensors based on conducting polymer composites: Review. *Chem. Phys. Lett.* **2021**, *776*, 138703.
(52) Park, H.; Kim, D.-H.; Ma, B. S.; Shin, E.; Kim, Y.; Kim, T.-S.; Kim, F. S.; Kim, I.-D.; Kim, B. J. High-Performance, Flexible NO_2 Chemiresistors Achieved by Design of Imine-Incorporated n-Type Conjugated Polymers. *Adv. Sci.* **2022**, *9* (14), 2200270.
(53) Maity, A.; Ghosh, B. Fast response paper based visual color change gas sensor for efficient ammonia detection at room temperature. *Sci. Rep.* **2018**, *8* (1), 16851.
(54) Oh, S.; Kang, S.; Cativo, M. H. M.; Yang, M.; Chung, S.-H.; Kim, J.; Bouffard, J.; Hong, S.; Park, S.-J. Long-Range Order Self-Assembly of Conjugated Block Copolymers at Inclined Air-Liquid Interfaces. *ACS Appl. Mater. Interfaces* **2020**, *12* (4), 5099−5105.
(55) Oh, S.; Yang, M.; Kang, S.; Chung, S.-H.; Bouffard, J.; Hong, S.; Park, S.-J. Binary Self-Assembly of Conjugated Block Copolymers and Quantum Dots at the Air-Liquid Interface into Ordered Functional Nanoarrays. *ACS Appl. Mater. Interfaces* **2019**, *11* (31), 28538−28545.

https://doi.org/10.1021/acsami.3c11940
ACS Appl. Mater. Interfaces 2023, 15, 51753−51762